Science Advances
AAAS

advances.sciencemag.org/cgi/content/full/6/24/eaaz7748/DC1

Supplementary Materials for

Marangoni flows drive the alignment of fibrillar cell-laden hydrogels

Bryan A. Nerger, P.-T. Brun, Celeste M. Nelson*

*Corresponding author. Email: celesten@princeton.edu

Published 12 June 2020, *Sci. Adv.* **6**, eaaz7748 (2020)
DOI: 10.1126/sciadv.aaz7748

The PDF file includes:

Other Supplementary Material for this manuscript includes the following:

(available at advances.sciencemag.org/cgi/content/full/6/24/eaaz7748/DC1)

Supplementary Materials

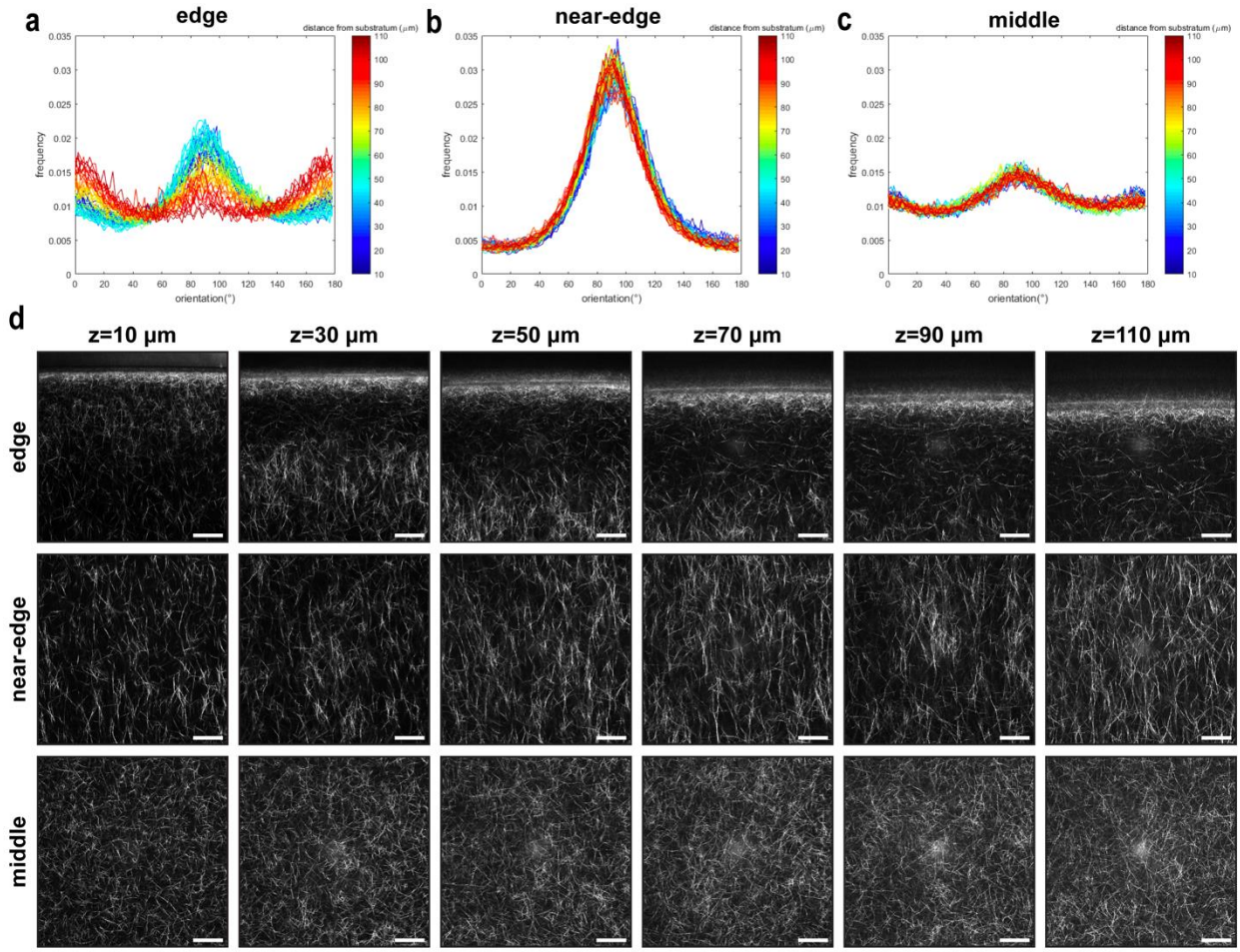

Fig. S1. Collagen fiber alignment in the edge region of the droplet varies with distance from the substratum. Plots showing the frequency of collagen fiber orientation as a function of distance from the glass substratum for the a) edge, b) near-edge, and c) middle regions of interest. d) Representative CRM images showing the fiber orientation as a function of distance above the glass substratum. Scale bars represent 50 μm. For all data in the figure, collagen solutions (pH 11) were gelled at controlled RH using a saturated solution of $MgCl_2$ (RH~31%) on UVO-treated glass.

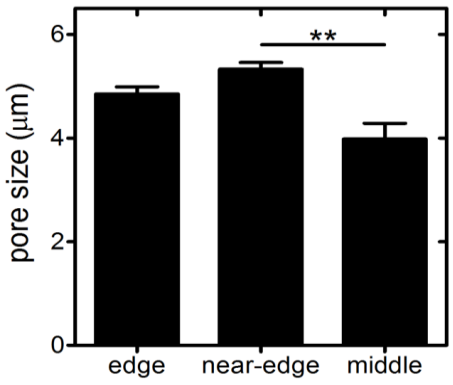

Fig. S2. Pore size varies spatially throughout the droplet. Pore size in the edge, near-edge, and middle regions of drop-cast collagen gels. For all data in the figure, collagen solutions (pH 11) were gelled at controlled RH using a saturated solution of $MgCl_2$ (RH~31%) on UVO-treated glass. **$p \leq 0.01$.

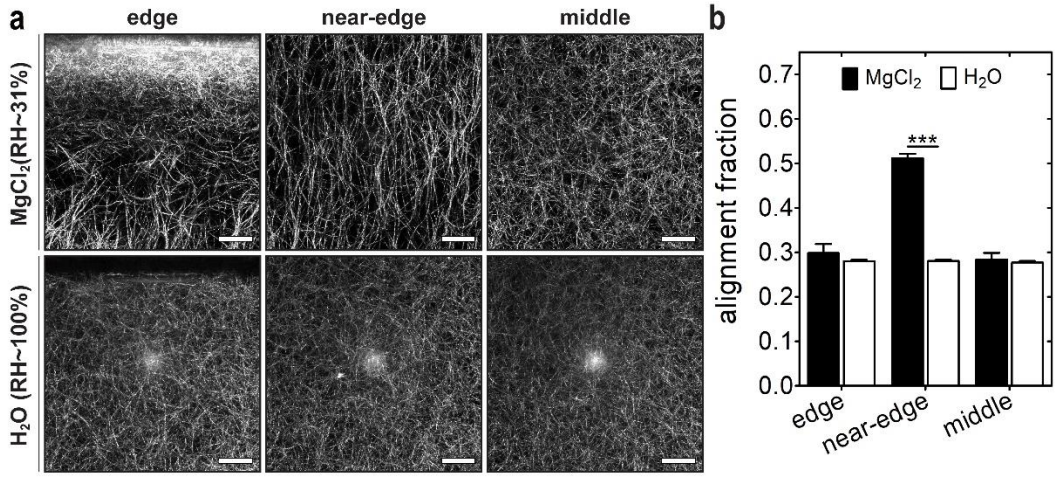

Fig. S3. Collagen fibers are randomly oriented in the absence of Marangoni flow. a) Representative CRM images and b) alignment fraction of drop-cast networks of collagen

that self-assembled in the presence of a saturated solution of $MgCl_2$ (RH~31%) or water (RH~100%). Collagen solutions (pH 11) were gelled on UVO-treated glass. ***$p \leq 0.001$.

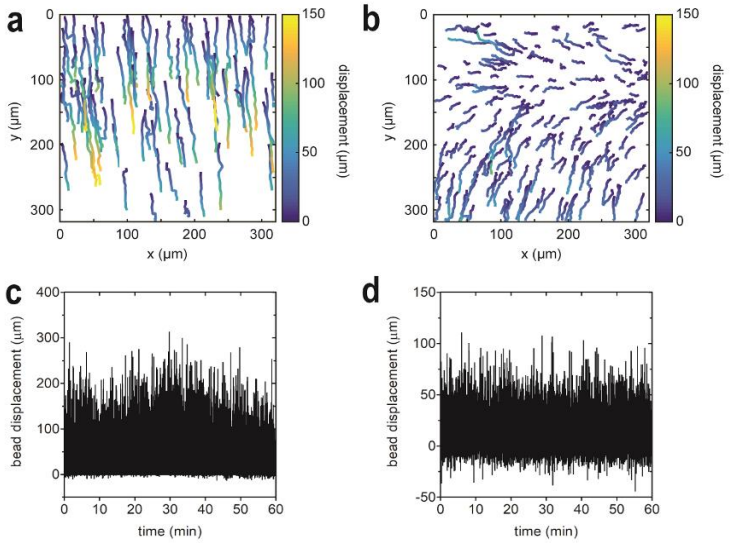

Fig. S4. Patterns of flow in evaporating droplets of PBS. Single-bead trajectories color-coded based on bead displacement for the a) near-edge and b) edge regions of an evaporating droplet of PBS. The first 500 bead trajectories that exceeded 10 frames in length in each region of interest are plotted. Radial bead displacement in the c) near-edge and d) edge region of an evaporating droplet of PBS as a function of time. For all data in the figure, collagen solutions were gelled at controlled RH using a saturated solution of $MgCl_2$ (RH~31%) on UVO-treated glass.

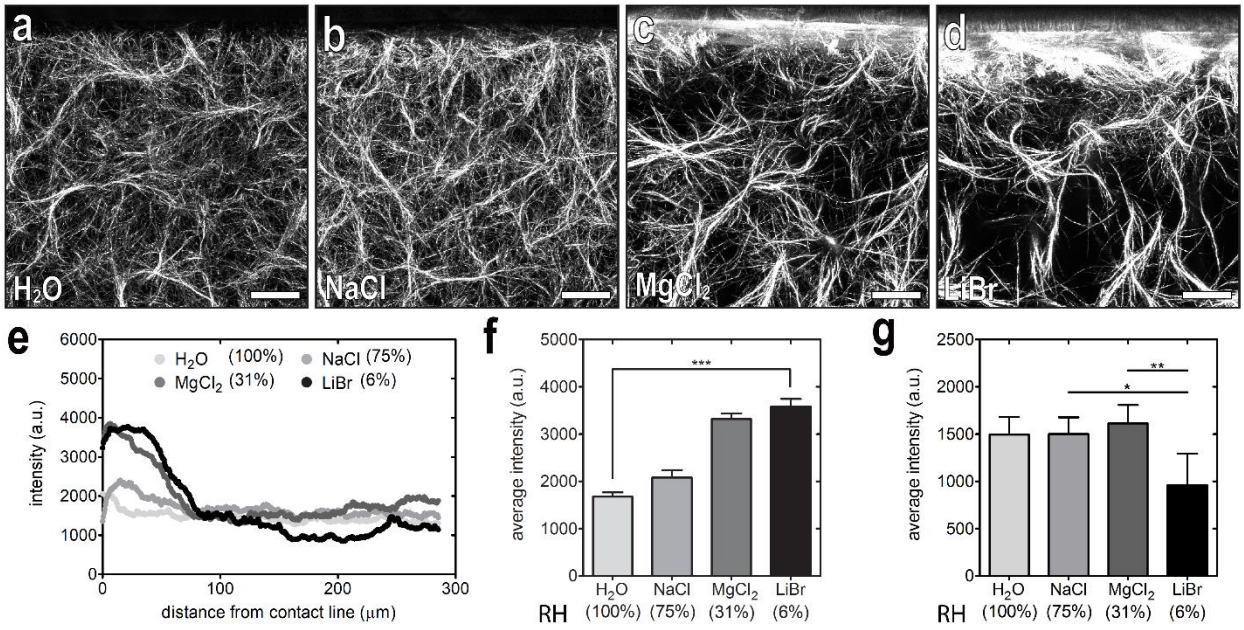

Fig. S5. Collagen accumulation at the droplet edge increases with decreasing RH. Representative CRM images of drop-cast networks of collagen that self-assembled at RH levels dictated by a) water (RH~100%) and saturated solutions of b) NaCl (RH~75%), c) $MgCl_2$ (RH~31%), and d) LiBr (RH~6%). e) Intensity of collagen fibers as a function of distance from the contact line of a self-assembled droplet of collagen. Average intensity of collagen fibers within f) 50 μm and g) 200-250 μm of the droplet contact line. The RH is denoted next to the label for each saturated salt solution. Scale bars represent 50 μm. For all data in the figure, collagen solutions were gelled on UVO-treated glass. *$p \leq 0.05$; **$p \leq 0.01$; ***$p \leq 0.001$.

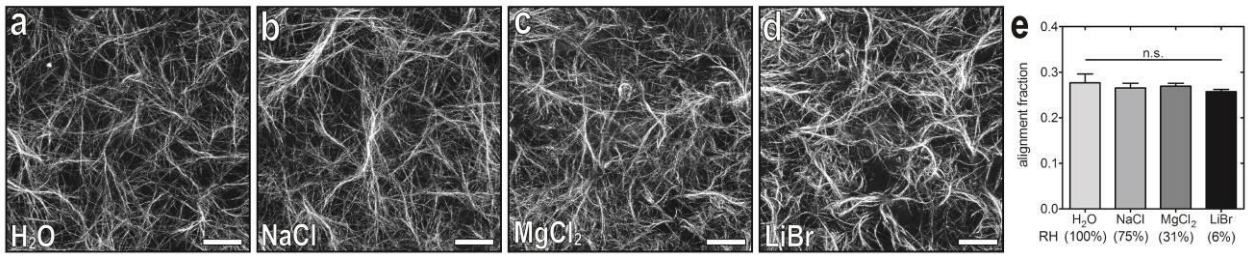

Fig. S6. RH does not affect collagen fiber alignment in the middle region of droplets. Representative CRM images of the middle region of droplets of collagen that self-assembled at RH levels dictated by a) water (RH~100%) and saturated solutions of b)

NaCl (RH~75%), c) $MgCl_2$ (RH~31%), or d) LiBr (RH~6%). e) Alignment fraction in the middle region of droplets of collagen as a function of RH. The RH is denoted next to the label for each saturated salt solution. Scale bars represent 50 μm. For all data in the figure, collagen solutions were gelled on UVO-treated glass. n.s., not significant.

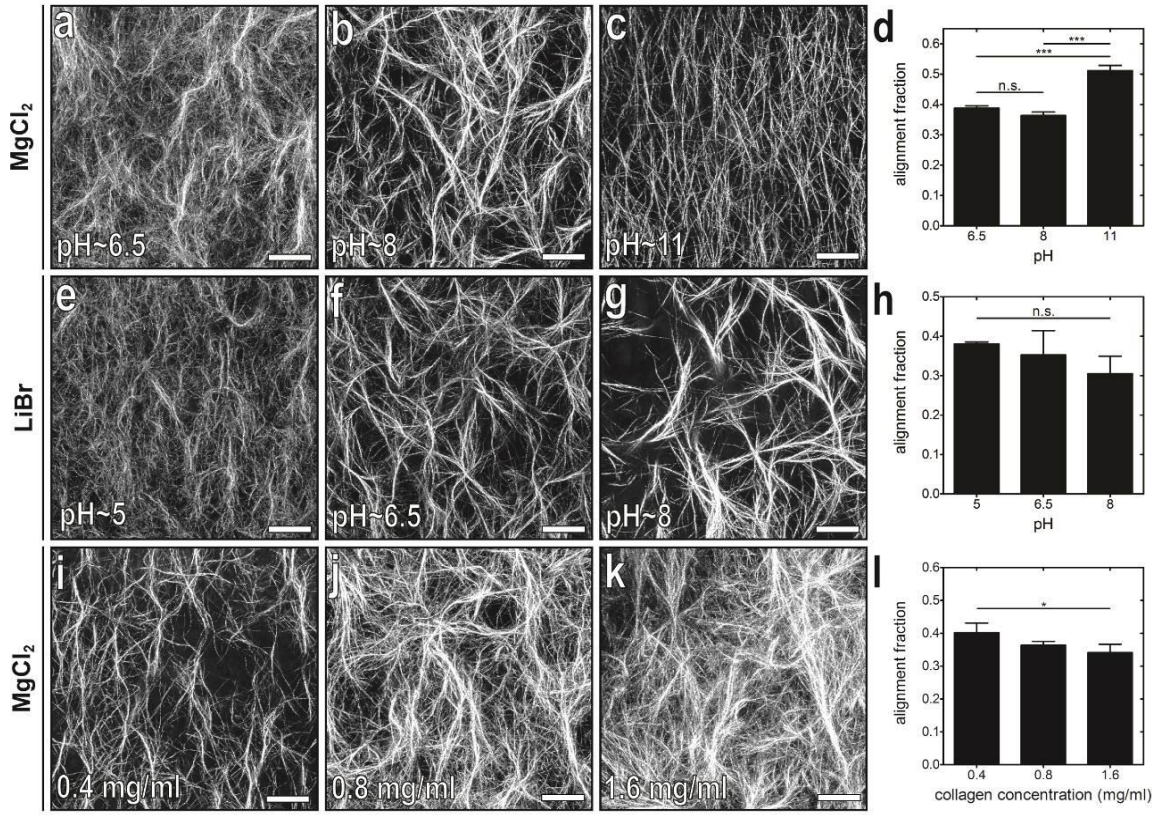

Fig. S7. Concentration and pH affect collagen fiber alignment. Representative CRM images in the near-edge region of droplets of collagen self-assembled at a pH of a) 6.5, b) 8, or c) 11. d) Alignment fraction of collagen fibers in the near-edge region of droplets that were incubated at different pH. Representative CRM images in the near-edge region of droplets of collagen self-assembled at a pH of e) 5, f) 6.5, or g) 8. h) Alignment fraction of collagen fibers in the near-edge region of droplets that were incubated at different pH. Representative CRM images in the near-edge region of droplets at a collagen concentration of i) 0.4 mg/ml, j) 0.8 mg/ml, or k) 1.6 mg/ml. l) Alignment fraction of collagen fibers in the near-edge region of droplets that were incubated at different collagen

concentrations. RH was controlled using a saturated solution of $MgCl_2$ (RH~31%) (a-d and i-l) or LiBr (RH~6%) (e-h). Scale bars represent 50 μm. For all data in the figure, collagen solutions were gelled on UVO-treated glass. *$p \leq 0.05$; ***$p \leq 0.001$; n.s., not significant.

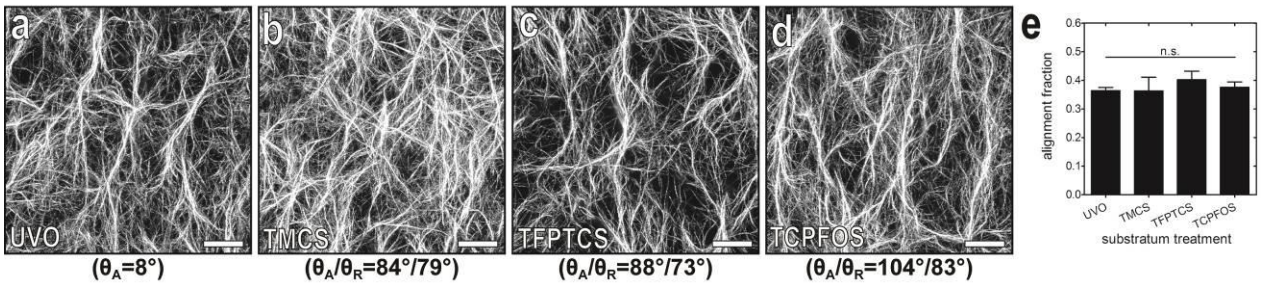

Fig. S8. Surface hydrophobicity does not significantly impact collagen fiber alignment in the near-edge region of evaporating droplets of collagen. Representative CRM images of the near-edge region of droplets of collagen on glass substrata treated with a) UVO, b) TMCS, c) TFPTCS, or d) TCPFOS. e) Alignment fraction of collagen fibers in the near-edge region of droplets of collagen that were drop cast onto each of the different surfaces. Advancing (θ_A) and receding (θ_R) contact angle data adapted from (*40*). RH was controlled using a saturated solution of $MgCl_2$ (RH~31%). Scale bars represent 50 μm. n.s., not significant.

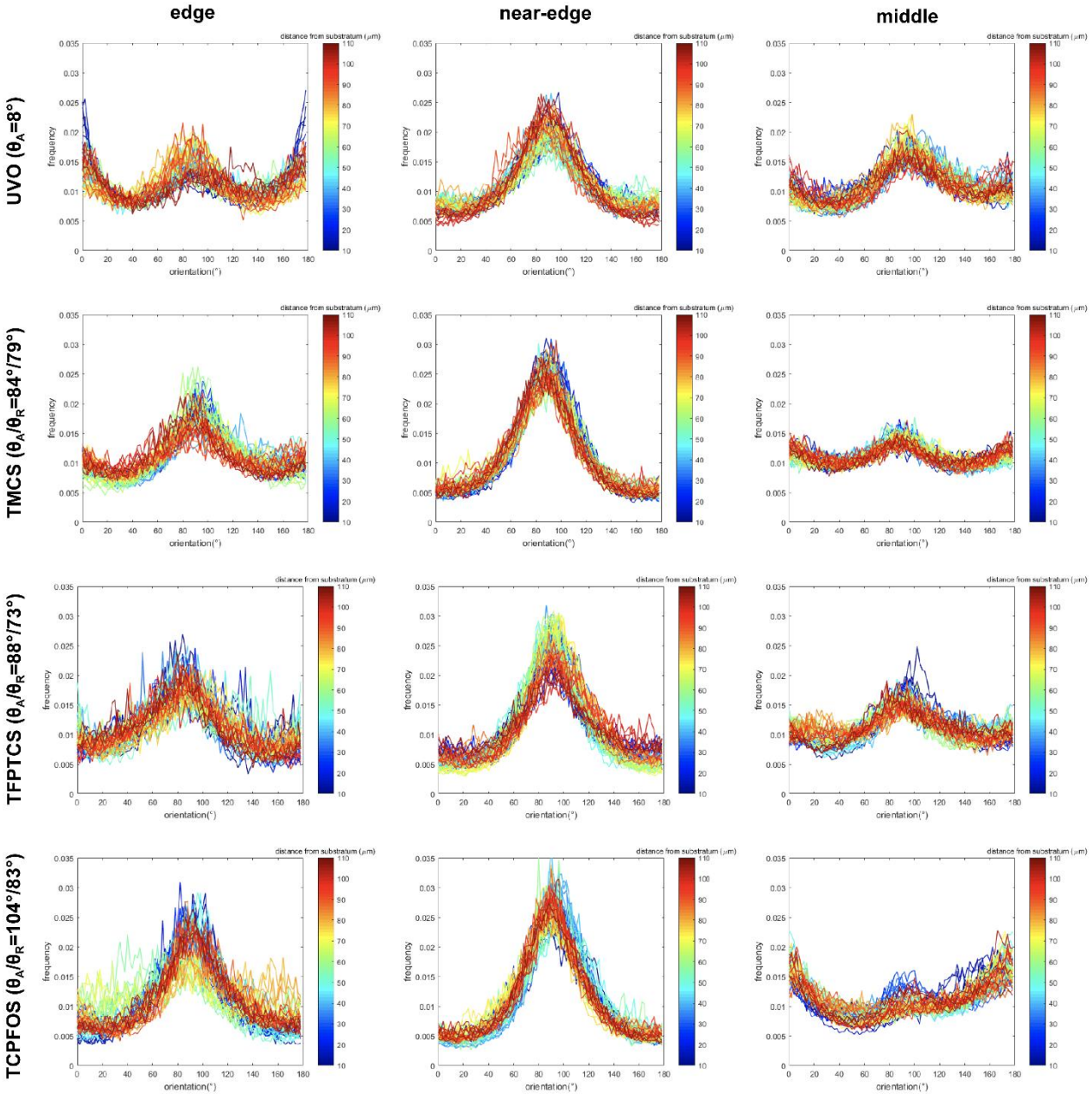

Fig. S9. Surface chemistry affects collagen fiber alignment in the edge region of the droplet. Plots showing the frequency of collagen fiber orientation as a function of distance from the glass substratum for the edge, near-edge, and middle regions of interest. Droplets were drop cast onto glass substratum treated with UVO, TMCS, TFPTCS, or TCPFOS. Advancing (θ_A) and receding (θ_R) contact angle data adapted from (*40*). For all data in the figure, collagen solutions were gelled at controlled RH using a saturated solution of $MgCl_2$ (RH~31%).

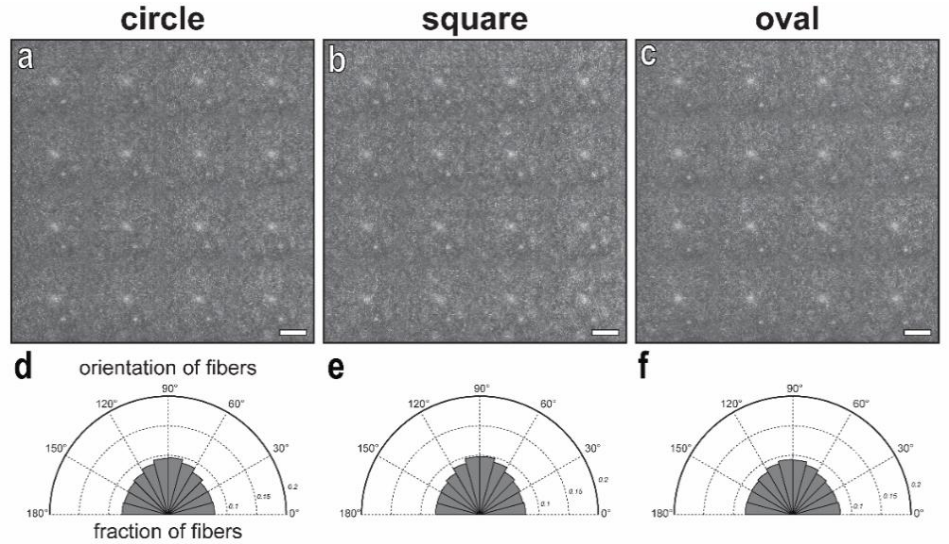

Fig. S10. Droplet geometry does not affect collagen fiber orientation in the absence of Marangoni flow. Representative CRM images of the middle region of a) circular, b) square, and c) oval droplets of collagen that were self-assembled in the presence of water (RH~100%). 16 CRM images were stitched together in order to show the orientation of collagen fibers throughout the middle region of the droplets. Scale bars represent 100 μm. Orientation of collagen fibers in the middle region of d) circular, e) square, and f) oval droplets of collagen. For all data in the figure, collagen solutions (pH 11) were gelled on UVO-treated glass.

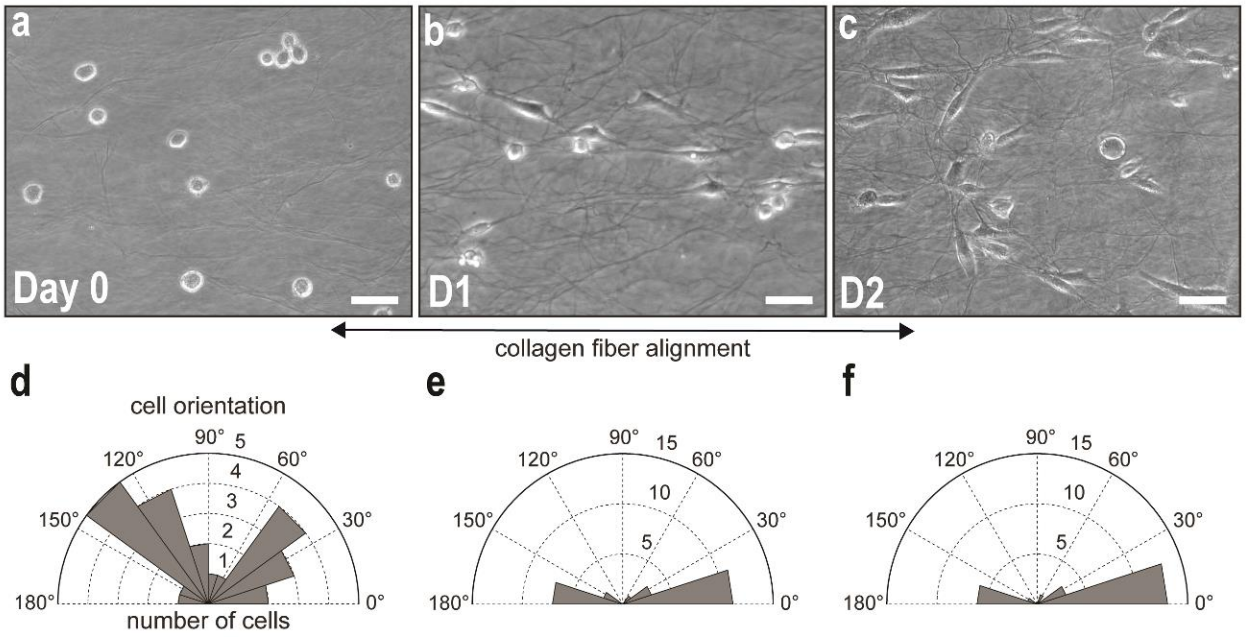

Fig. S11. Human breast cancer cells orient in the direction of collagen fiber alignment. Representative phase-contrast images of human breast cancer cells embedded in self-assembled droplets of collagen a) immediately, b) ~24 h, and c) ~48 h after self-assembly. Scale bars represent 50 μm. RH was controlled using a saturated solution of $MgCl_2$ (RH~31%) and collagen solutions were gelled on UVO-treated glass. Plots of cell orientation d) immediately, e) ~24 h, and f) ~48 h after self-assembly. 24 cells were analyzed for each condition.

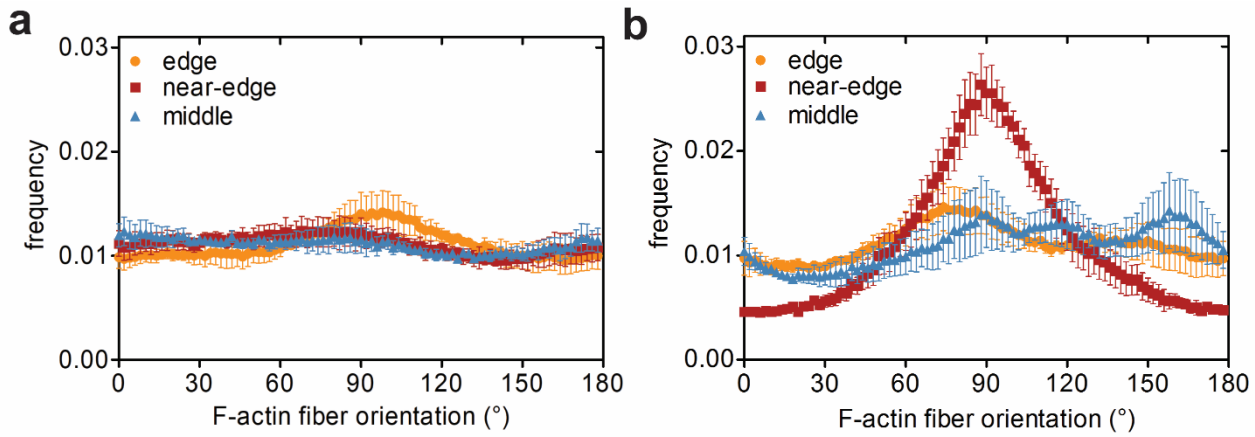

Fig. S12. F-actin fibers orient in the direction of collagen fiber alignment throughout the droplet. Plot showing the orientation of F-actin fibers in skeletal muscle cells in the edge, near-edge, and middle regions of droplets of collagen that were self-assembled in the presence of a) water (RH~100%) or b) a saturated solution of $MgCl_2$ (RH~31%). The concentration of collagen was 2 mg/ml for panel (a) and ~2.3 mg/ml for panel (b). For all data in the figure, collagen solutions were gelled on UVO-treated glass.

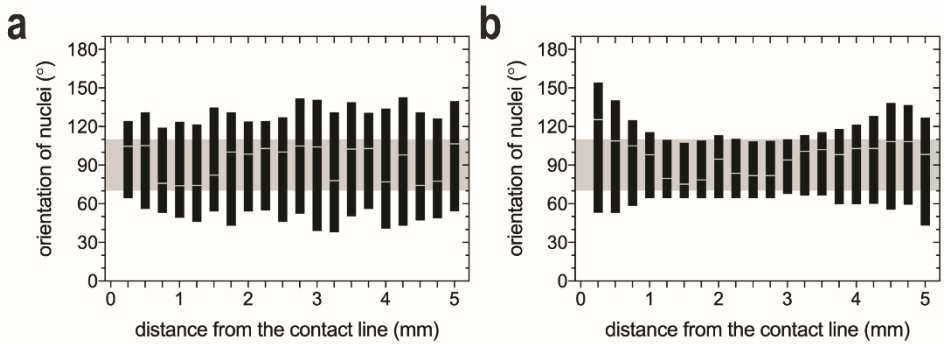

Fig. S13. Evaporating droplets of collagen pattern the orientation of skeletal muscle cells. Box plots of the orientation of nuclei as a function of distance from the contact line for drop-cast collagen gels (~2 mg/ml) self-assembled in the presence of a) water (RH~100%) (n=8099) or b) a saturated solution of $MgCl_2$ (RH~31%) (n=10251). N represents the number of nuclei analyzed. The black boxes depict the median and the interquartile range. The shaded region corresponds to nuclei that are orientated within 20° of the radial direction in the droplet. For all data in the figure, collagen solutions were gelled on UVO-treated glass.

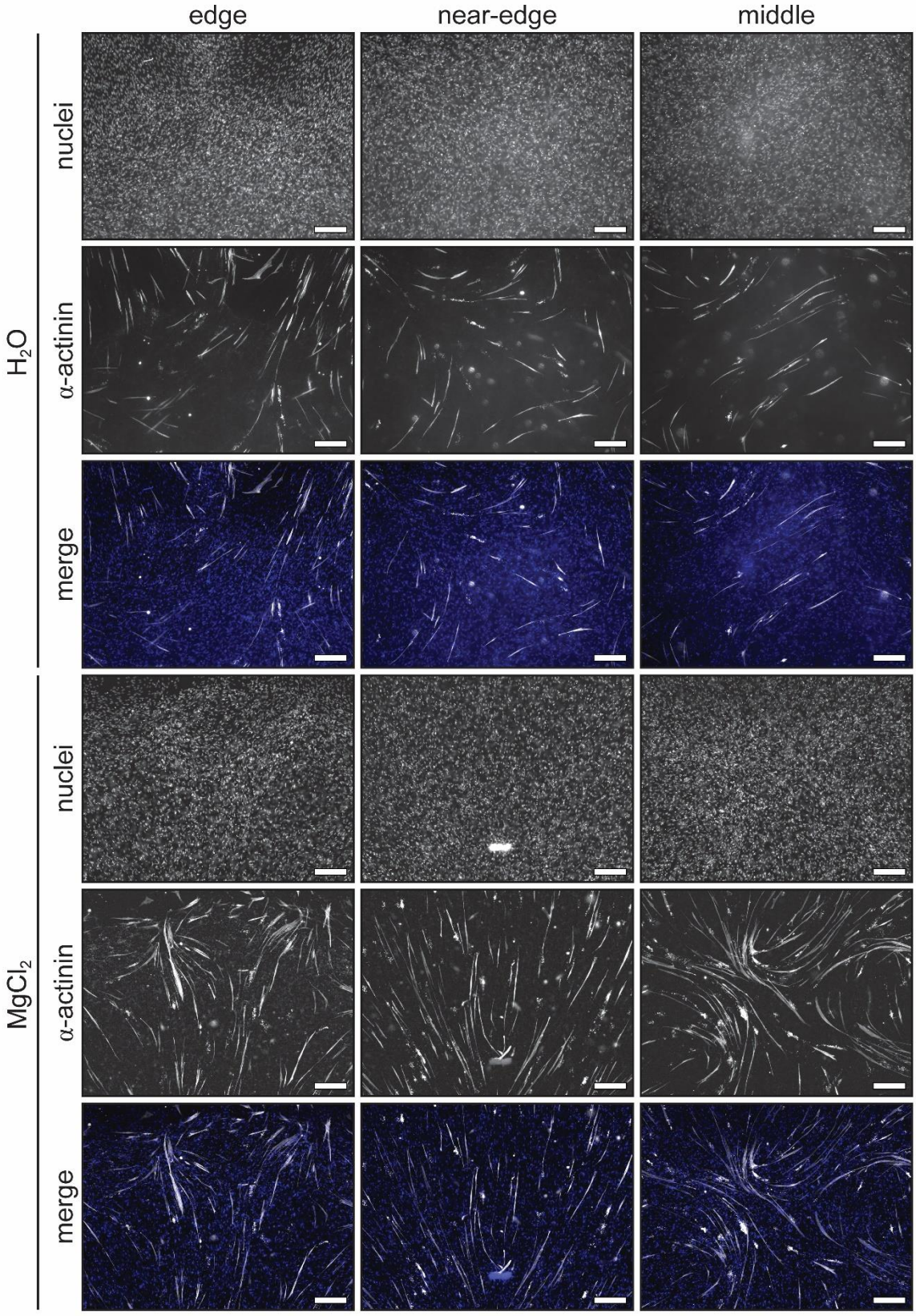

Fig. S14. Sarcomeric structures orient in the direction of collagen fiber alignment throughout the droplet. Representative immunofluorescence images of skeletal muscle cells in the edge, near-edge, or middle regions of droplets of collagen after 4 days in

differentiation medium. Cells are stained with Hoechst 33342 to label nuclei (blue) and an antibody against sarcomeric α-actinin (gray). Scale bars represent 250 μm. The concentration of collagen was 2.0 mg/ml or 2.13 mg/ml for droplets of collagen that were self-assembled in the presence of water (RH~100%) or a saturated solution of $MgCl_2$ (RH~31%), respectively. For all data in the figure, collagen solutions were gelled on UVO-treated glass.

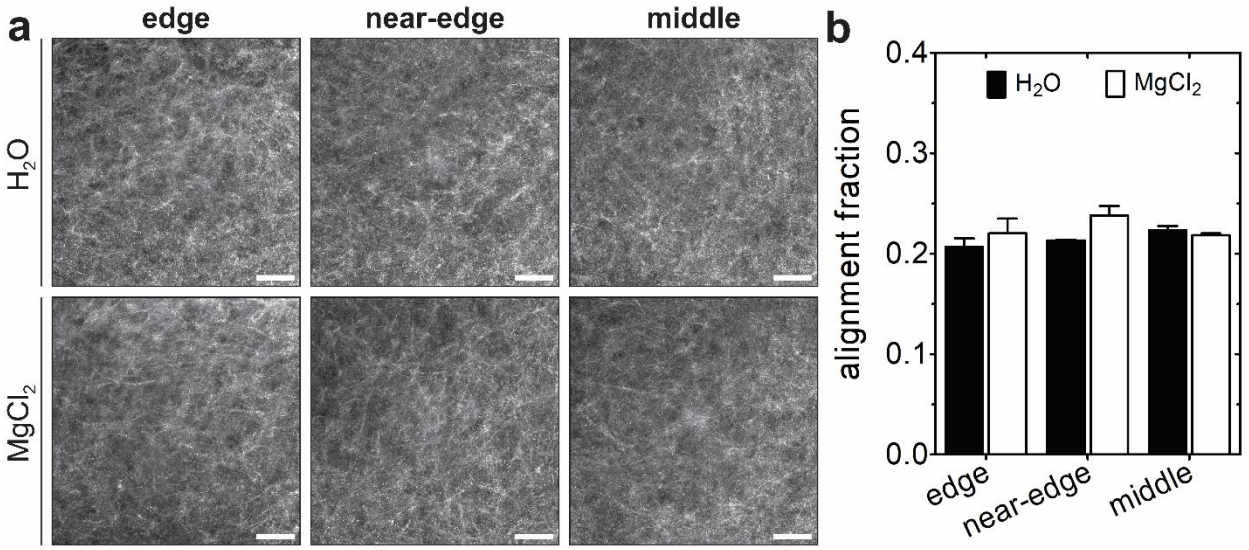

Fig. S15. Skeletal muscle cells distort collagen fiber alignment patterns in each region of interest of the droplet. a) Representative CRM images of the edge, near-edge, and middle regions of droplets of collagen containing skeletal muscle cells that were self-assembled in the presence of water (RH~100%) or $MgCl_2$ (RH~31%). The concentration of collagen was 2 mg/ml, and droplets were cultured for ~8 days before imaging. Scale bars represent 50 μm. b) Alignment fraction of collagen fibers in each region of the droplets. For all data in the figure, collagen solutions were gelled on UVO-treated glass.

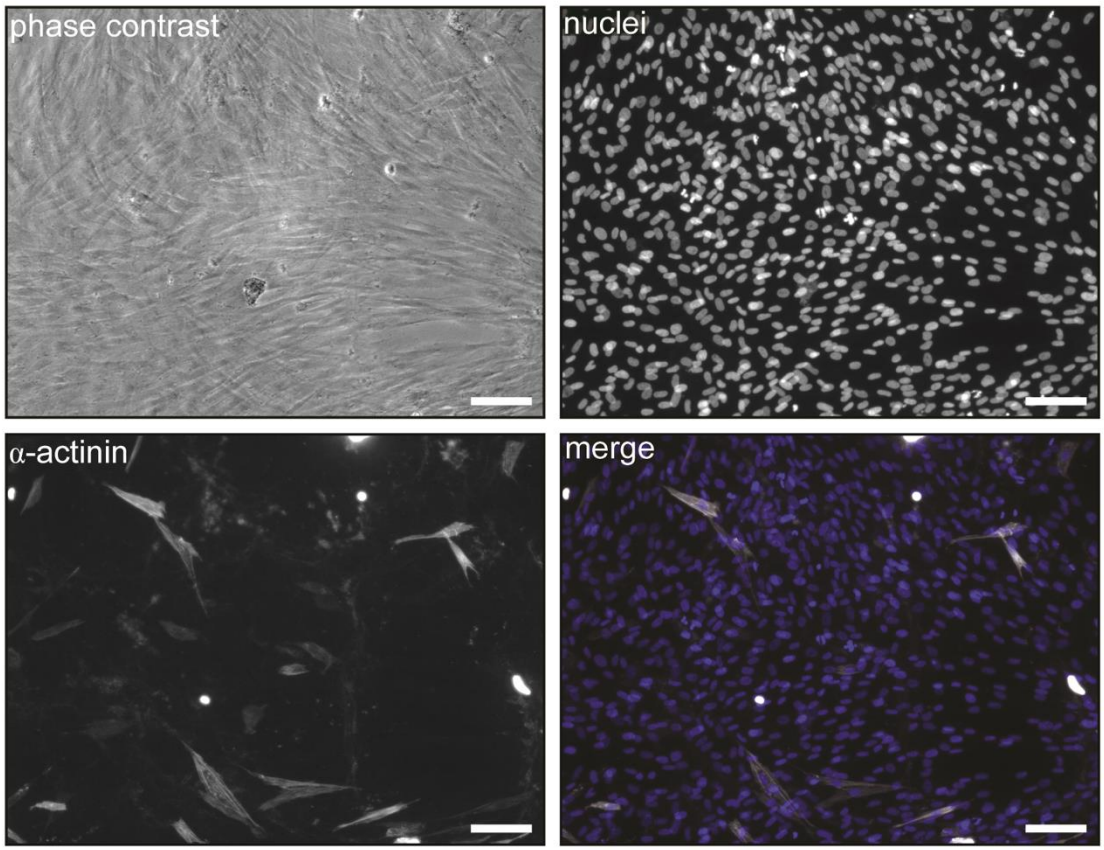

Fig. S16. Sarcomeric structures are randomly organized when skeletal muscle cells are cultured on top of a glass substratum. Representative phase contrast and fluorescence images of skeletal muscle cells after 3 days in differentiation medium. Cells are stained with Hoechst 33342 to label nuclei (blue) and phalloidin to label F-actin (gray). Scale bars represent 100 μm.

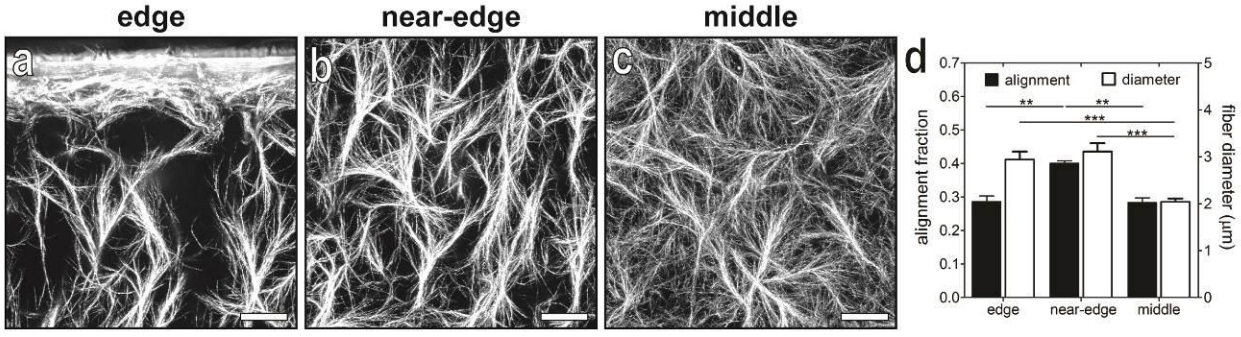

Fig. S17. Evaporation-driven flow generates aligned networks of collagen in droplets of collagen-Matrigel. Representative CRM images of the a) edge, b) near-edge, or c)

middle regions of droplets of collagen-Matrigel. d) Alignment fraction of collagen fibers in each region of interest. Scale bars represent 50 μm. RH was controlled using a saturated solution of $MgCl_2$ (RH~31%) and collagen solutions were gelled on UVO-treated glass. $^{**}p \leq 0.01$; $^{***}p \leq 0.001$.

Movie S1. Representative time-lapse CRM videos of bead movements in the edge, near-edge, and middle regions of drop-cast collagen. RH was controlled using a saturated solution of $MgCl_2$ (RH~31%) and collagen solutions were gelled on UVO-treated glass.

Movie S2. Representative time-lapse CRM videos of collagen fiber self-assembly in the edge, near-edge, and middle regions of drop-cast collagen. RH was controlled using a saturated solution of $MgCl_2$ (RH~31%) and collagen solutions were gelled on UVO-treated glass.

Movie S3. Representative time-lapse CRM videos of collagen fiber self-assembly and bead movements in the near-edge region of drop-cast collagen. RH was controlled using a saturated solution of $MgCl_2$ (RH~31%) and collagen solutions were gelled on UVO-treated glass.

Table S1. Weissenberg number calculations.

Collagen structure	Collagen diameter (μm)	Collagen length (μm)	Average velocity (μm/s)	Shear rate (1/s)	Relaxation time (s)	Wi
monomer	0.0015	0.3	1.6937	0.033874	0.0008	2.71E-05
fiber	0.15596	14.571	1.6937	0.033874	132.73	4.50